PAPER

Check for updates

Facile fabrication of hierarchical textures for substrate-independent and durable superhydrophobic surfaces†

Yuchun He,[a] Lingxiao Wang,[a] Tingni Wu,[a] Zhipeng Wu,[a] Yu Chen[a] and Kai Yin ⓘD *[a,b]

On account of their wide range of applications in self-cleaning, anti-icing, frost suppression, *etc.*, super-hydrophobic surfaces have attracted considerate attention. However, most of the superhydrophobic surfaces can only be prepared on the surfaces of specific materials and are easily damaged in the case of friction. In this work, we propose a facile method to achieve superhydrophobicity on various substrate surfaces. By femtosecond laser direct processing, micron-level grooves and protrusions are constructed on substrates to form a protective layer. Then, the substrates covered by polytetrafluoroethylene (PTFE) were scanned to make the surfaces of the substrates superhydrophobic. Since the PTFE micro–nano-particles are evenly distributed on the grooves and protrusions, the surfaces exhibit robust superhydrophobicity with excellent anti-friction performance that is independent of the substrate properties. This work provides an efficient and environmentally friendly path for achieving robust superhydrophobic surfaces on various substrates.

1. Introduction

The superhydrophobic property means that the water contact angle (WCA) of the surface is larger than 150° and the sliding angle is less than 10°.[1,2] Considering its extensive application prospects in fundamental research and practical applications, this special phenomenon has attracted much attention since it was discovered.[3–8] Specific applications of superhydrophobic surfaces include but are not limited to the following scenarios. Iced metal surfaces could affect their service life. However, due to their ultra-low adhesion to water, the superhydrophobic metal surfaces are difficult to be frozen, and the ice easily slips down after melting into water droplets, which can effectively solve the problem of icing.[9–12] Mold grows easily on cellulose-based materials such as wood and paper in water or humid environments, which adversely affects the practicability of the materials. When they are covered with a superhydrophobic surface, it is like a waterproof layer on the surfaces and the moisture resistance of these materials will be greatly

improved.[13–17] In medical treatment, ordinary hemostatic materials are easily wetted by blood and have a single function. Superhydrophobic hemostatic materials can limit blood wetting, prevent blood loss and significantly reduce bacterial adhesion.[18] A surface enhanced Raman scattering (SERS) platform can detect toxins in liquids. However, due to the random diffusion of liquids into the sensor, the SERS platform is poor in the ultra-trace detection and quantitative analysis of toxins. After the SERS platform superhydrophobization, the random diffusion of liquids is limited, and the ability of the ultra-trace detection and quantitative analysis of the platform is greatly improved.[19] Passive radiation cooling materials play an important role in reducing energy consumption, but their application is limited by the surface pollution in the actual environment. Because of its self-cleaning function, the surface contamination of superhydrophobic radiation cooling materials has been well solved.[18] In addition, superhydrophobic surfaces have important applications in nanogenerators, super-capacitors, chemical catalysis, *etc.*[20–23]

Because of the great potential of superhydrophobic surfaces in scientific investigations, a lot of studies on how to obtain superhydrophobic surfaces have been performed by many researchers over the years. For instance, Lo Porto *et al.* etched the PTFE surface with oxygen plasma and modified it.[24] The superhydrophobic surface can be obtained in one step, which is fast and pollution-free. Wu *et al.* modified various nano-particles and vinyl triethoxysilane under gravity and pressure to get superhydrophobic surfaces on most solid substrates.[25]

[a]Hunan Key Laboratory of Nanophotonics and Devices, School of Physics and Electronics, Central South University, Changsha 410083, China.
E-mail: kaiyin@csu.edu.cn
[b]The State Key Laboratory of High Performance and Complex Manufacturing, College of Mechanical and Electrical Engineering, Central South University, Changsha 410083, China

Schutzius *et al.* dispersed exfoliated graphite nanosheets in weakly alkaline aqueous solution and then mixed them with a commercial polyolefin dispersion to prepare a water-based, fluorine-free dispersion, and this dispersion can produce superhydrophobic layers on a variety of substrates.[26] However, most of the present methods to prepare superhydrophobic surfaces have some limitations, such as substrate-dependence, complicated steps, environmental pollution, time-consuming nature and so on,[27–32] and the method of obtaining superhydrophobic surfaces only on one or several specific materials cannot adapt to the wide application scenarios of superhydrophobic surfaces. Moreover, superhydrophobic surfaces usually work in complex situations with friction. Therefore, a fast, simple, and environment-friendly method for obtaining friction-resistant superhydrophobic surfaces on various substrates is urgently needed.

Herein, we report a simple, rapid, and substrate-free method for preparing friction-resistant superhydrophobic surfaces *via* femtosecond laser direct writing.[33–37] The micron grid structure is first constructed on the substrate surface, and then PTFE nanoparticles are deposited on the substrate by femtosecond laser second scanning. Both fluorines from PTFE films and two-scale micro/nanostructures are used to improve the hydrophobicity of the samples.[38] The laser-treated samples still have good superhydrophobicity after the friction tests, which shows excellent stability.

2. Experimental section

2.1 Preparation of superhydrophobic surfaces

The PTFE films (~0.03 mm) were bought from Taizhou Chengguang Plastic Industry Co., Ltd (China), and the silicon wafers were bought from Zhejiang Lijing Optoelectronics Technology Co., Ltd (China). Quartz glass, paper, and stainless steel were all purchased from local markets.

This method can be realized on various solid substrates by adjusting appropriate processing parameters. Taking quartz glass as an example, the laser was focused on the upper surface of quartz glass, the output power of the femtosecond laser (HR-Femto-IR-50-40B, Huaray, China) was adjusted to 8 W, and the frequency and the pulse width were 100 kHz and 350 fs, respectively. The galvanometer system (basiCube 10, Scanlab, Germany) was controlled by the software on a computer to process quartz glass with a scanning speed of 0.5 mm s^{-1} and a scanning distance of 0.1 mm, and the "#" shaped grid structure was constructed on the surface of quartz glass in the X-direction first and then in the Y-direction.[39] Next, a PTFE film with a thickness of 0.03 μm was tightly covered on the "#" shaped glass, and the laser was refocused on the upper surface of PTFE. In the second scanning, the femtosecond laser power was 5 W, which controlled the galvanometer to deposit PTFE along the X-direction at a scanning speed of 100 mm s^{-1} and a scanning spacing of 0.05 mm. Afterward, we removed the PTFE film and replaced it with a new PTFE film. The same parameters were used to scan the PTFE film along the

Y-direction, the PTFE nanoparticles were deposited on the substrate, and finally, the PTFE film could be removed (glass: 8 W, 100 kHz, 100 μm, 0.5 mm s^{-1}; stainless steel: 8 W, 100 kHz, 100 μm, 10 mm s^{-1}; silicon slice: 6.5 W, 100 kHz, 100 μm, 50 mm s^{-1}, paper: 4 W, 100 kHz, 100 μm, 200 mm s^{-1}; PTFE film: 5 W, 100 kHz, 50 μm, 100 mm s^{-1}).

2.2 Characterization

Firstly, due to the poor conductivity of some samples, a low vacuum coating instrument (EM ACE200, Leica, Germany) was used to plate a thin platinum film on the sample surfaces to improve the conductivity of the samples. Then, the surface morphologies of the samples were observed using a scanning electron microscope (SEM; MIRA3, LMU, Tescan, Czech Republic), and the element distributions of the samples were analyzed quantitatively using a supporting energy dispersion spectrometer (EDS; Tescan, Czech Republic). A laser scanning confocal microscope (CLSM; Axio LSM700, Zeiss, Germany) was used to observe the three-dimensional morphologies and cross-sectional profiles of the sample surfaces, and the WCAs at five different positions on the same sample surface were measured with a contact angle meter (Biolin Scientific, Finland) to reduce the error.

3. Results and discussion

3.1 Design and realization of superhydrophobic surfaces

In order to obtain superhydrophobic surfaces on a variety of substrates concisely and quickly, the femtosecond laser direct processing method was selected because of its eco-friendly nature, high efficiency, high precision, and large instantaneous energy.[40–42] The schematic of the processing procedure is shown in Fig. 1a. (I) We used a femtosecond laser to process the structure surfaces with a "#" shaped path and (II) then the PTFE film was tightly covered on the laser-treated structure surfaces, and the PTFE micro/nanoparticles were deposited on the "#" shaped micro/nanostructure surfaces *via* femtosecond laser second scanning.[43,44] As we all know, PTFE is dangerous when it is heated up to 400°. But in this work, when the PTFE film is treated with the femtosecond laser, its maximum temperature is only 83.3°, so that the whole process is always in a safe state (Fig. S1 in ESI†). Fig. 1b and c show the static WCA images of quartz glass, stainless steel, silicon wafer, and paper before and after processing. The water droplets are completely spread out on the pristine glass, showing a minor arc on stainless steel and silicon wafer, but a major arc on paper.[45] At the same time, the shapes of water droplets on the surfaces of the laser-treated samples are almost completely spherical. It is obvious that the wettability of the four materials is different, and the corresponding WCAs are ~23.2°, 69.7°, 73.5°, and 118.7°, respectively, while the laser-treated surfaces show superhydrophobicity, and the WCAs are ~158.9°, 156.3°, 162.6°, and 165.6°, respectively (Fig. 1d). In addition, our method demonstrates overwhelming overall performances over its other counterparts in substrate-indepen-
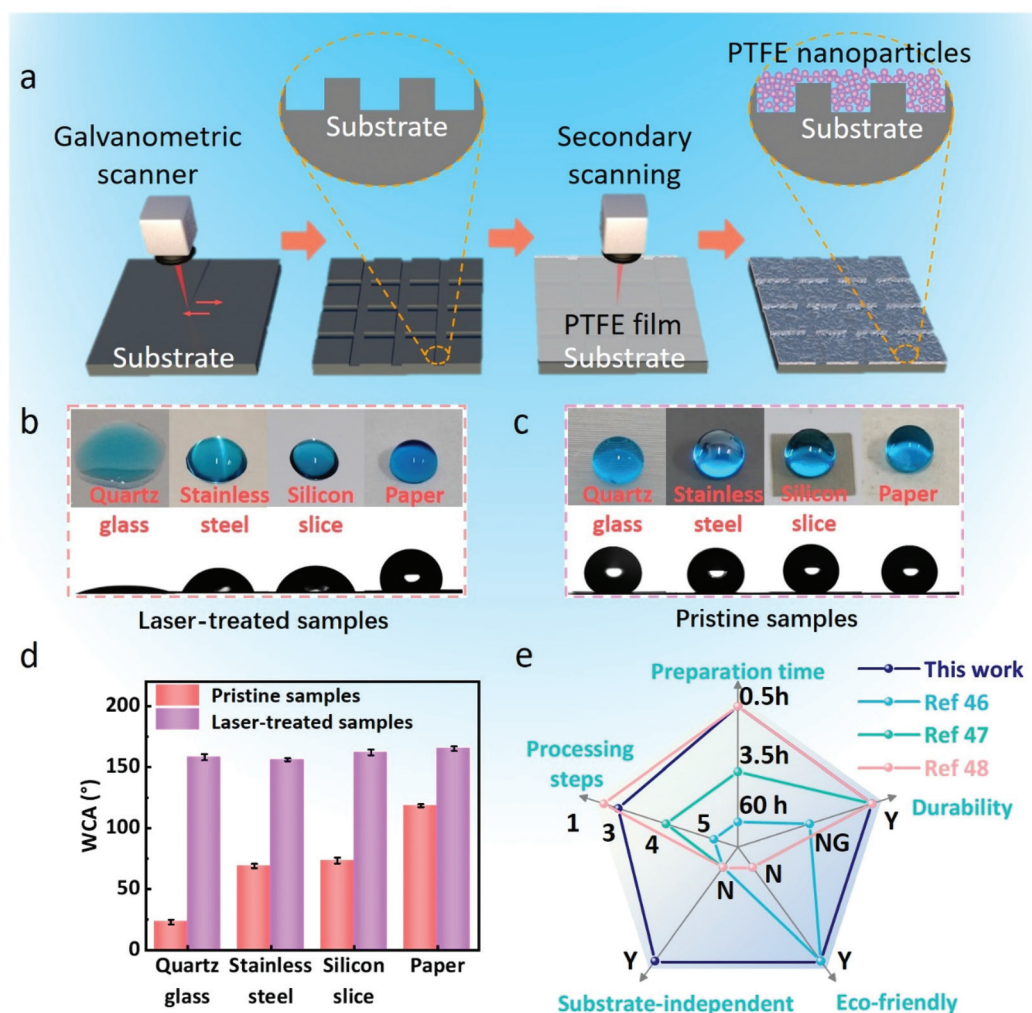
Fig. 1 (a) Schematic illustration of the fabrication procedure of the robust superhydrophobic surface; (b and c) water droplets are placed on the pristine and laser-treated samples of four substrates (quartz glass, stainless steel, silicon slice, and paper); for convenience of observation, water has been stained with methylene blue; (d) comparison of WCAs of the pristine and laser-treated samples; (e) comparison between our method and other similar methods in terms of substrate-independence, durability, processing steps, preparation time and environmental protection.

dence, durability, preparation time, and eco-friendliness (Fig. 1e).[46–48]

3.2 Surface topography

To investigate the reason for the superhydrophobicity of the laser-treated structures, we characterized their surface morphology by SEM. It can be seen that the pristine structures of quartz glass, stainless steel, and silicon wafer are relatively smooth and flat, and the surface of pristine paper displays the morphology of staggered distribution of fibers (Fig. S2 in ESI†). According to the existing theory, the hydrophobicity of a solid surface depends on the roughness and free energy of the surface. The hydrophobic properties will be further enhanced by higher surface roughness or lower surface free energy. Based on the above reasons, several laser-treated surfaces are in a "#" grid shape. Because the first scanning spacing of the femtosecond laser is twice the second scanning spacing, the grooves with one being deep and one shallow are staggered. After second scanning, a large number of micro/nano-

particles are found distributed in the bulges and grooves on the substrate surfaces, and clusters formed by micro/nanoparticles are observed under high magnifications, which are deposited on the substrate surfaces and filled with the micro/nanostructures (Fig. 2a–d). Meanwhile, we characterized the element composition and distribution on the surfaces of these structures after processing. It can be clearly seen that the elements such as carbon, oxygen, and fluorine are distributed on the surfaces of the four substrates evenly, and the distribution is consistent with the "#" shape contour. In particular, the atomic element percentage of fluorine on each substrate's surface is in the range of 29.3% to 38.2%, which exhibits fairly good consistency. Due to the limited field depth of EDS, the element distribution in the grooves cannot be clearly displayed, so the grooves in each element distribution diagram are black (Fig. 2e–h).

Furthermore, we also used LCM to characterize the 3D morphology and cross-section profile of the structures of laser-treated surfaces.[49–51]

Fig. 2 (a–d) SEM images of quartz glass, stainless steel, silicon wafer, and paper after femtosecond laser ablation; (e–h) EDS spectra and elemental mapping of laser-treated quartz glass, stainless steel, silicon wafer, and paper, respectively.

This shows that the groove's depths in the four laser-treated samples are about 30–150 μm; the great difference in depths is due to the various ablation thresholds of each material. Furthermore, the distribution of grooves shows obvious periodicity as shown in Fig. 3a–d. Based on the above results, we can preliminarily infer the reason for the superhydrophobic characteristics of the structures after processing: the PTFE micro/nanoparticles deposited on the substrates have low surface free energy because they are rich in fluorine, which makes the substrates have high hydrophobicity. At the same time, these micro/nanoparticles were combined with the "#" shaped structure on the substrate surface to form a micro/ nano two-scale structure. In consequence, the specific surface area of the substrate surface was greatly increased, the hydro-

phobicity of the substrate surface was further improved, and the substrate surface finally showed superhydrophobic characteristics.

3.3 Wettability characterization and durability tests

The obtained superhydrophobic surfaces were also further verified, as shown in Fig. 4. For more clarity, quartz glass was selected as an example. A dropper was used to carry about 4 μL water droplets to drop on the laser-treated glass surface, the droplets were moderately compressed after they came in contact with the structure surface, and finally the dropper was slowly lifted (Fig. 4a, Movie S1 in the ESI†). The structure surface remained free of water droplets, which proved the superhydrophobicity and low adhesion of the structured
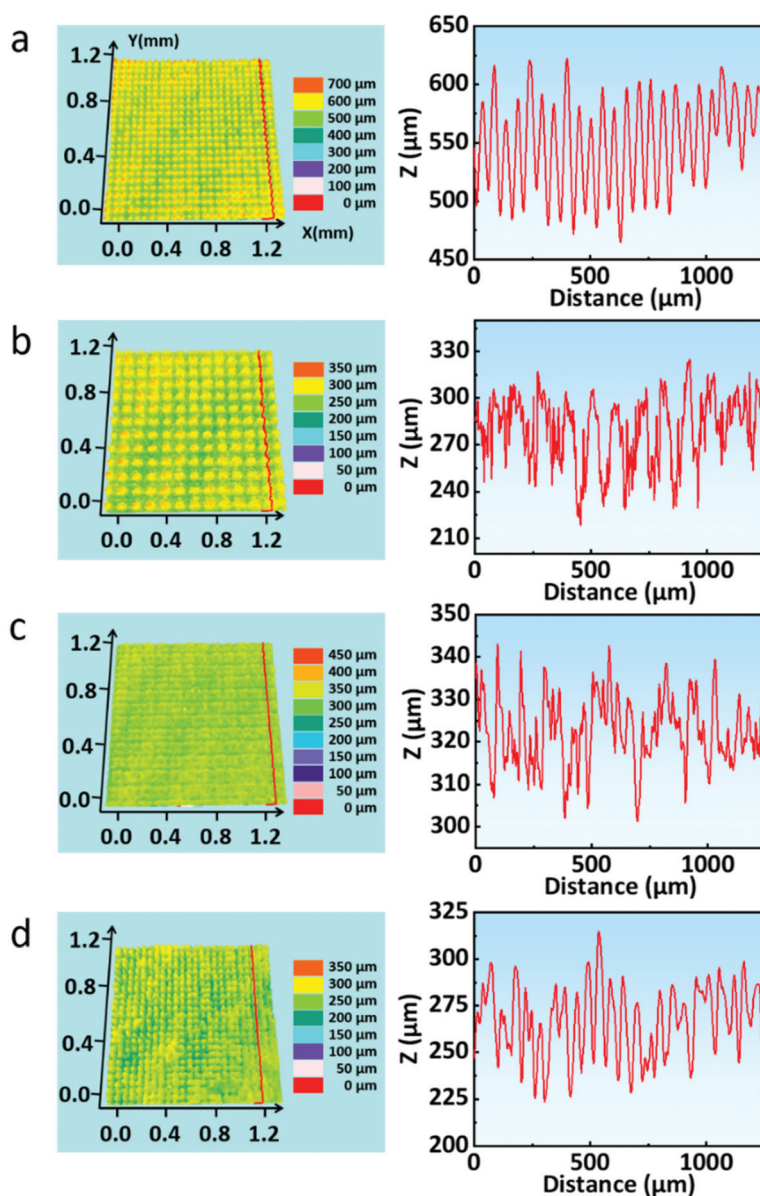
Fig. 3 (a–d) 3D surface topography and the cross-sectional profile of laser-treated quartz glass, stainless steel, silicon slice, and paper, respectively.

surface. Concurrently, the water droplet could easily roll on the surface with a tilted angle of ~2.6° (Fig. 4b, Movie S2 in the ESI†). Fig. 4c shows the bouncing test of a water droplet on the treated glass surface.[52,53] When the water droplet just touched the treated surface, it was recorded as 0 ms. After coming in contact with the surface, the water droplet began to spread on the interface until the maximum diameter was reached in about 7 ms, then began to shrink, completed the contraction and gradually jumped up in about 16 ms. This is also a reflection of the superhydrophobicity and low adhesion of the treated surface (Movie S3 in the ESI†). As illustrated in Fig. 4d, we placed an appropriate amount of dust on the pristine glass and the laser-treated glass, respectively. Then water was dripped slowly on these surfaces with a dropper. On account

of the hydrophilicity and high adhesion of the pristine glass, the water droplets adhere to the glass surface and do not roll-off. Naturally, the dust on the pristine glass was still retained. In contrast, because of its superhydrophobicity and low adhesion, the water droplets were close to a complete sphere on the laser-treated glass surface, carried the dust, and rolled down into the dish quickly, and the cleaned surface of the glass was finally observed. This is one of the important applications of superhydrophobic surfaces, that is, the self-cleaning function of the material surface (Movies S4 and S5 in the ESI†).[54–57] Moreover, the durability tests of the superhydrophobic performance were also conducted. We repeatedly pasted and tore off transparent tape on the laser-treated glass, and it could be found that it still maintained superhydrophobicity

Fig. 4 (a) Dynamic adhesion behavior of water droplets coming in contact and leaving the laser-treated glass surface; (b) water droplets roll down from the laser-treated glass with an inclination angle of ~2.6°; (c) pictures of the continuity of the bouncing behavior of water droplets on the laser-treated glass surface; (d) the self-cleaning performance of the pristine glass surface and laser-treated glass; (e) adhesive tape is used to adhere on and tear the laser-treated glass surface and the WCAs of laser-treated surface after multiple cycles; (f) the WCAs of the laser-treated quartz glass at different temperatures (10 °C−90 °C).

for 10 cycles, and the WCAs were greater than 151°, which proved that the laser-treated glass had a certain anti-glue viscosity (Fig. 4e).[58] Fig. 4f shows that the laser-treated glass is superhydrophobic in the temperature range of 10 °C to 90 °C. In order to further test the anti-friction ability and practicability of the samples, samples loaded with weight (50 g) are rubbed on sandpaper to simulate scratches that may be

encountered in daily life.[59–62] With the laser-treated surface facing down, the sample slides along with the weight on the sandpaper by pushing it with tweezers (Fig. 5a). On comparing the SEM images of the laser-treated surfaces before and after friction, it can be found that the surface layer of the structures after friction turns smoother while the morphology in the groove changes slightly (Fig. 5b).
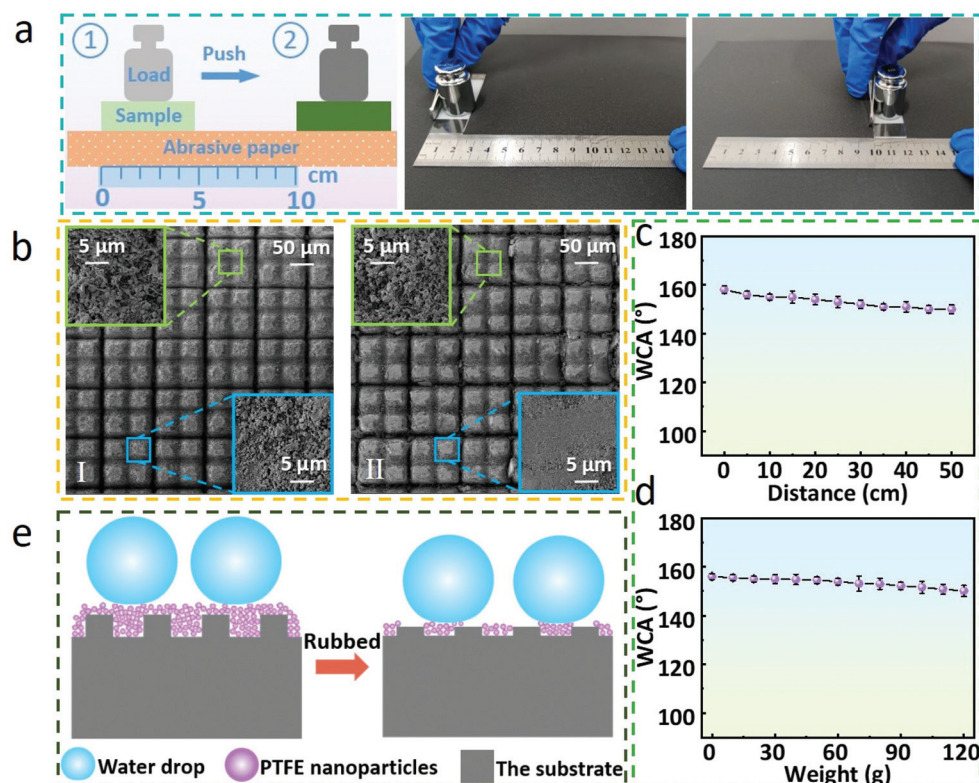
Fig. 5 (a) Schematic illustration and experimental diagram of the sandpaper friction test; (b) SEM images of the laser-treated glass surface before and after the friction; an enlarged view of a groove is shown in the upper left corner and an enlarged view of a protrusion is shown in the lower right corner; (c) the WCAs of various friction distances of laser-treated glass loaded with 50 g; (d) the change of WCAs on the laser-treated glass with a friction distance of 10 cm with the different load weights; and (e) schematic illustration of the principle that the laser-treated samples after friction still have superhydrophobicity.

By measuring the WCAs of multiple groups of samples loaded with weights rubbed on sandpaper for different distances, it was observed that the laser-treated glass still maintained superhydrophobicity with a friction distance of ~50 cm, and the WCA was 152.2°. On the other hand, the WCAs of laser-treated glass with various weights ranging from 0 to 120 g after rubbing on sandpaper for 10 cm were also measured. The results demonstrate convincingly that the laser-treated glass also maintains superhydrophobicity within these loading ranges. In this regard, combined with the theories mentioned above, the following explanations are discussed. As displayed in Fig. 5e, the laser-treated glass shows superhydrophobicity derived from PTFE micro/nanoparticles and double-scale structures formed on the surface before friction. Simultaneously, the majority of the PTFE micro/nanoparticles in the grooves are retained (Fig. 5b and Fig. S3 in the ESI†), retaining the superhydrophobicity of laser-treated glass surface after multiple frictions.

4. Conclusion

In summary, a simple and efficient method for preparing robust superhydrophobic surfaces on a variety of substrates is proposed, which is based on the femtosecond laser engraving of substrates and laser induced PTFE deposition. Four different kinds of laser-treated samples have WCAs greater than 150° and remain superhydrophobic after proper friction. Their superhydrophobicity comes from the two-scale micro/nanostructures formed by PTFE nanoparticles and micron structures on the substrates, as well as the low surface free energy of PTFE nanoparticles. More importantly, these superhydrophobic surfaces have good self-cleaning function and mechanical stability. This substrate-independent, robust superhydrophobic surface has broad application prospects due to its simple preparation.

Conflicts of interest

The authors declare no competing financial interests.

Acknowledgements

References

1 Z. Wu, K. Yin, J. Wu, Z. Zhu, J. A. Duan and J. He, *Nanoscale*, 2021, **13**, 2209–2226.

2 F. Wang, J. Pi, F. Song, R. Feng, C. Xu, X. L. Wang and Y. Z. Wang, *Chem. Eng. J.*, 2020, **381**, 122539.

3 W. Bai, J. Xu, M. Guan, Y. He, Y. Xu and J. Lin, *J. Taiwan Inst. Chem. Eng.*, 2019, **95**, 71–77.

4 X. Zhao, D. S. Park, J. Choi, S. Park, S. A. Soper and M. C. Murphy, *J. Colloid Interface Sci.*, 2020, **574**, 347–354.

5 Z. Ye, S. Li, S. Zhao, L. Deng, J. Zhang and A. Dong, *Chem. Eng. J.*, 2021, **420**, 127680.

6 M. Wang, Y. Zi, J. Zhu, W. Huang, Z. Zhang and H. Zhang, *Chem. Eng. J.*, 2021, **417**, 129265.

7 A. K. Singh and J. K. Singh, *Prog. Org. Coat.*, 2019, **131**, 301–310.

8 A. R. Esmaeili, N. Mir and R. Mohammadi, *J. Colloid Interface Sci.*, 2020, **573**, 317–327.

9 L. Cao, A. K. Jones, V. K. Sikka, J. Wu and D. Gao, *Langmuir*, 2009, **25**, 12444–12448.

10 G. Jiang, L. Chen, S. Zhang and H. Huang, *ACS Appl. Mater. Interfaces*, 2018, **10**, 36505–36511.

11 C. Peng, S. Xing, Z. Yuan, J. Xiao, C. Wang and J. Zeng, *Appl. Surf. Sci.*, 2012, **259**, 764–768.

12 R. Pan, H. Zhang and M. Zhong, *ACS Appl. Mater. Interfaces*, 2021, **13**, 1743–1753.

13 J. Zhao, W. Zhu, X. Wang, L. Liu, J. Yu and B. Ding, *ACS Nano*, 2020, **14**, 1045–1054.

14 A. S. Anjum, K. C. Sun, M. Ali, R. Riaz and S. H. Jeong, *Chem. Eng. J.*, 2020, **401**, 125859.

15 L. Song, X. F. Zhang, Z. Wang, Y. Bai, Y. Feng and J. Yao, *Adv. Mater. Interfaces*, 2020, **7**, 202001166.

16 Y. Zhao, D. Qu, T. Yu, X. Xie, C. He, D. Ge and L. Yang, *Chem. Eng. J.*, 2020, **385**, 123860.

17 Z. Yi, B. Zhao, M. Liao and Z. Qin, *Coatings*, 2020, **10**, 10090847.

18 Z. Li, A. Milionis, Y. Zheng, M. Yee, L. Codispoti, F. Tan, D. Poulikakos and C. H. Yap, *Nat. Commun.*, 2019, **10**, 5562.

19 X. Li, H. K. Lee, I. Y. Phang, C. K. Lee and X. Y. Ling, *Anal. Chem.*, 2014, **86**, 10437–10444.

20 B. Y. Liu, C. H. Xue, H. M. Zhong, X. J. Guo, H. D. Wang, H. G. Li, M. M. Du, M. C. Huang, R. X. Wei, L. G. Song, B. Chang and Z. Wang, *J. Mater. Chem. A*, 2021, **9**, 24276–24282.

21 W. Xu, H. Zheng, Y. Liu, X. Zhou, C. Zhang, Y. Song, X. Deng, M. Leung, Z. Yang, R. X. Xu, Z. L. Wang, X. C. Zeng and Z. Wang, *Nature*, 2020, **578**, 392–396.

22 J. Sung, H. M. Lee, G. H. Yoon, S. Bae and H. So, *Int. J. Precis. Eng. Manuf. - Green Technol.*, 2022, DOI: **10.1007/s40684-022-00418-y**.

23 X. Zhang, T. Zhou, J. Liu, R. Wang, W. Hu and L. Liu, *Appl. Surf. Sci.*, 2021, **540**, 148337.

24 C. Lo Porto, R. Di Mundo, V. Veronico, I. Trizio, G. Barucca and F. Palumbo, *Appl. Surf. Sci.*, 2019, **483**, 60–68.

25 Y. Wu, S. Jia, Y. Qing, S. Luo and M. Liu, *J. Mater. Chem. A*, 2016, **4**, 14111–14121.

26 T. M. Schutzius, I. S. Bayer, J. Qin, D. Waldroup and C. M. Megaridis, *ACS Appl Mater Interfaces*, 2013, **5**, 13419–13425.

27 Z. Dai, G. Chen, S. Ding, J. Lin, S. Li, Y. Xu and B. Zhou, *Adv. Funct. Mater.*, 2020, **31**, 202008574.

28 D. Dey, N. Chandra Murmu and P. Banerjee, *RSC Adv.*, 2019, **9**, 7469–7478.

29 J. Huang, S. Lyu, Z. Chen, S. Wang and F. Fu, *J. Colloid Interface Sci.*, 2019, **536**, 349–362.

30 S. Jia, H. Chen, S. Luo, Y. Qing, S. Deng, N. Yan and Y. Wu, *Appl. Surf. Sci.*, 2018, **455**, 115–122.

31 S. Jia, X. Lu, S. Luo, Y. Qing, N. Yan and Y. Wu, *Chem. Eng. J.*, 2018, **348**, 212–223.

32 S. Kim, H. J. Hwang, H. Cho, D. Choi and W. Hwang, *Chem. Eng. J.*, 2018, **350**, 225–232.

33 Z. Luo, K. Yin, X. Dong and J. A. Duan, *J. Phys. D: Appl. Phys.*, 2018, **51**, 185104.

34 J. Wu, K. Yin, M. Li, Z. Wu, S. Xiao, H. Wang, J. A. Duan and J. He, *Nanoscale*, 2020, **12**, 4077–4084.

35 K. Yin, S. Yang, X. Dong, D. Chu, J.-A. Duan and J. He, *Appl. Phys. Lett.*, 2018, **112**, 243701.

36 K. Yin, Z. Wu, J. Wu, Z. Zhu, F. Zhang and J. A. Duan, *Appl. Phys. Lett.*, 2021, **118**, 211905.

37 J. Long, P. Fan, D. Gong, D. Jiang, H. Zhang, L. Li and M. Zhong, *ACS Appl. Mater. Interfaces*, 2015, **7**, 9858–9865.

38 S. Wang, Y. Wang, Y. Zou, G. Chen, J. Ouyang, D. Jia and Y. Zhou, *ACS Appl. Mater. Interfaces*, 2020, **12**, 35502–35512.

39 D. Wang, Q. Sun, M. J. Hokkanen, C. Zhang, F. Y. Lin, Q. Liu, S. P. Zhu, T. Zhou, Q. Chang, B. He, Q. Zhou, L. Chen, Z. Wang, R. H. A. Ras and X. Deng, *Nature*, 2020, **582**, 55–59.

40 K. Ahmmed, C. Grambow and A.-M. Kietzig, *Micromachines*, 2014, **5**, 1219–1253.

41 K. Sugioka and Y. Cheng, *Appl. Phys. Rev.*, 2014, **1**, 041303.

42 S. Yang, K. Yin, D. Chu, J. He and J. A. Duan, *Appl. Phys. Lett.*, 2018, **113**, 203701.

43 C. Chen, Z. Huang, S. Zhu, B. Liu, J. Li, Y. Hu, D. Wu and J. Chu, *Adv. Sci.*, 2021, **8**, e2100701.

44 S. Jiang, Y. Hu, H. Wu, Y. Zhang, Y. Zhang, Y. Wang, Y. Zhang, W. Zhu, J. Li, D. Wu and J. Chu, *Adv. Mater.*, 2019, **31**, e1807507.

45 I. Torun, N. Celik, M. Ruzi and M. S. Onses, *Surf. Coat. Technol.*, 2021, **405**, 126543.

46 Z. Xiao, Z. Li, H. Guo, Y. Liu, Y. Wang, H. Yin, X. Li, J. Song, L. D. Nghiem and T. He, *Desalination*, 2019, **466**, 36–43.

47 L. B. Boinovich, A. M. Emelyanenko, K. A. Emelyanenko and E. B. Modin, *ACS Nano*, 2019, **13**, 4335–4346.

48 J. Liu, Y. Sun, X. Zhou, X. Li, M. Kappl, W. Steffen and H. J. Butt, *Adv. Mater.*, 2021, **33**, e2100237.

49 T. Wu, Z. Wu, Y. He, Z. Zhu, L. Wang and K. Yin, *Chin. Opt. Lett.*, 2022, **20**, 033801.

50 S. Yang, K. Yin, J. Wu, Z. Wu, D. Chu, J. He and J. A. Duan, *Nanoscale*, 2019, **11**, 17607–17614.

51 S. Yang, Z. Zhu, Z. Wu, J. Wu and K. Yin, *Appl. Phys. Lett.*, 2020, **117**, 213701.

52 M. Hubert, D. Robert, H. Caps, S. Dorbolo and N. Vandewalle, *Phys. Rev. E: Stat., Nonlinear, Soft Matter Phys.*, 2015, **91**, 023017.

53 H. Wu, K. Jiang, Z. Xu, S. Yu, X. Peng, Z. Zhang, H. Bai, A. Liu and G. Chai, *Langmuir*, 2019, **35**, 17000–17008.

54 T. Zhu, Y. Cheng, J. Huang, J. Xiong, M. Ge, J. Mao, Z. Liu, X. Dong, Z. Chen and Y. Lai, *Chem. Eng. J.*, 2020, **399**, 125746.

55 Y. Mao, F. Wang, Y. Li, R. Guidoin, L. Wang and F. Wang, *Appl. Surf. Sci.*, 2020, **517**, 146104.

56 N. Yu, X. Xiao, Z. Ye and G. Pan, *Surf. Coat. Technol.*, 2018, **347**, 199–208.

57 S. K. Sethi and G. Manik, *Polym.-Plast. Technol. Eng.*, 2018, **57**, 1932–1952.

58 M. D'Acunzi, A. Sharifi-Aghili, K. I. Hegner and D. Vollmer, *iScience*, 2021, **24**, 102460.

59 M. Liu, Y. Luo and D. Jia, *ACS Appl. Mater. Interfaces*, 2020, **12**, 6677–6687.

60 K. Yin, J. Wu, Q. Deng, Z. Wu, T. Wu, Z. Luo, J. Jiang and J. A. Duan, *Chem. Eng. J.*, 2022, **434**, 134756.

61 K. Yin, L. Wang, Q. Deng, Q. Huang, J. Jiang, G. Li and J. He, *Nano-Micro Lett.*, 2022, **14**, 97.

62 J. A. Duan, X. Dong, K. Yin, S. Yang and D. Chu, *Appl. Phys. Lett.*, 2018, **113**, 203704.